PHYSICAL REVIEW D **84,** 084039 (2011)

Higher-dimensional puncture initial data

Miguel Zilhão,[1,*] Marcus Ansorg,[2] Vitor Cardoso,[3,4] Leonardo Gualtieri,[5] Carlos Herdeiro,[6] Ulrich Sperhake,[7,8,3] and Helvi Witek[3]

[1]*Centro de Física do Porto, Departamento de Física e Astronomia, Faculdade de Ciências da Universidade do Porto, Rua do Campo Alegre, 4169-007 Porto, Portugal*
[2]*Theoretisch-Physikalisches Institut, Friedrich-Schiller-Universität Jena, Max-Wien-Platz 1, D-07743 Jena, Germany*
[3]*Centro Multidisciplinar de Astrofísica—CENTRA, Departamento de Física, Instituto Superior Técnico—IST, Avenida Rovisco Pais 1, 1049-001 Lisboa, Portugal*
[4]*Department of Physics and Astronomy, The University of Mississippi, University, Mississippi 38677-1848, USA*
[5]*Dipartimento di Fisica, Università di Roma "Sapienza" & Sezione, INFN Roma1, P. A. Moro 5, 00185, Roma, Italy*
[6]*Departamento de Física da Universidade de Aveiro & I3N, Campus de Santiago, 3810-183 Aveiro, Portugal*
[7]*Institut de Ciències de l'Espai (CSIC-IEEC), Facultat de Ciències, Campus UAB, E-08193 Bellaterra, Spain*
[8]*California Institute of Technology, Pasadena, California 91125, USA*

(Received 8 August 2011; published 18 October 2011)

We calculate puncture initial data, corresponding to single and binary black holes with linear momenta, which solve the constraint equations of D-dimensional vacuum gravity. The data are generated by a modification of the pseudospectral code presented in [M. Ansorg, B. Bruegmann, and W. Tichy, Phys. Rev. D **70**, 064011 (2004).] and made available as the TWOPUNCTURES thorn inside the CACTUS computational toolkit. As examples, we exhibit convergence plots, the violation of the Hamiltonian constraint as well as the initial data for $D = 4, 5, 6, 7$. These initial data are the starting point to perform high-energy collisions of black holes in D dimensions.

DOI: 10.1103/PhysRevD.84.084039 PACS numbers: 04.25.D−

I. INTRODUCTION

Numerical relativity in higher-dimensional spacetimes could be a powerful tool to study a variety of physical concepts, such as the stability of black hole solutions and their interactions, as well as for producing phenomenological information of relevance for TeV gravity scenarios [1–3]. In such models, the fundamental Planck scale could be as low as 1 TeV. Thus, high-energy colliders, such as the Large Hadron Collider (LHC), may directly probe strongly coupled gravitational physics [4–9]. Indeed, in this scenario, particle collisions could produce black holes [6,7]. Moreover, the production of black holes at trans-Planckian collision energies (compared to the fundamental Planck scale) should be well-described by using classical general relativity extended to D dimensions (see [10], and references therein). Numerical simulations of high-energy black hole collisions in higher-dimensional spacetimes, then, could give an accurate estimate of the fractions of the collision energy and angular momentum that are lost in the higher-dimensional space by emission of gravitational waves; such information would be extremely important to improve the modeling of microscopic black hole production, and of the ensuing evaporation phase, which might be observed during LHC collisions.

The growing interest in dynamical aspects of higher-dimensional spacetimes led to the development of higher-dimensional numerical relativity [11–14] and to the production of the first black hole collisions in higher-dimensional spacetimes starting from rest [15,16], and, most recently, of black holes with initial boost [17].[1] Aside from their immediate relevance in the context of TeV gravity scenarios, high-energy collisions of black holes provide fertile ground for probing strong-field effects of general relativity, such as cosmic censorship, luminosity limits, hoop type conjectures, and zoom-whirl behavior [17–21].

The modeling of generic black hole or neutron-star spacetimes in the framework of Einstein's theory of general relativity requires a numerical treatment because of the enormous complexity of the equations in the absence of high degrees of symmetry. For such numerical modeling, the Einstein equations are cast as a time evolution or *initial value* problem as originally formulated by Arnowitt-Deser-Misner (ADM) [22] and reformulated by York [23]. Numerically generating a solution then consists of two basic steps: (i) the construction of initial data which satisfy the constraint equations and represent a realistic snapshot of the physical system under consideration and (ii) the evolution in time of these initial data. In this work, we will focus on the first step and provide a formalism for constructing initial data for black hole binaries with nonzero boosts in higher, $D \geq 5$, dimensional spacetimes.

*mzilhao@fc.up.pt

[1]These simulations start from superposed single boosted black hole data without application of a constraint-solving procedure; our work is motivated in part by providing initial data for a comparison and thus calibrating the impact of constraint violations.

Most work on the generation of initial data in $3+1$-dimensional general relativity is based on the York-Lichnerowicz split [24–27] which rearranges the degrees of freedom contained in the three-metric γ_{ij} and extrinsic curvature K_{ij} via a conformal transformation and a split of the curvature into trace and traceless part

$$\gamma_{ij} = \psi^4 \hat{\gamma}_{ij}, \tag{1.1}$$

$$K_{ij} = A_{ij} + \frac{1}{3}\gamma_{ij} K, \tag{1.2}$$

followed by a transverse-traceless decomposition of either the traceless extrinsic curvature A_{ij} or a conformally rescaled version $\hat{A}_{ij}$ thereof. For details of these *physical* or *conformal transverse-traceless* decompositions as well as the alternative *conformal thin-sandwich* formalism, we refer the reader to Cook's review [28], Alcubierre's book [29], and references therein.

One of the main advantages achieved with this decomposition is the decoupling of the momentum from the Hamiltonian constraint under the additional simplifying assumptions of conformal flatness, $\hat{\gamma}_{ij} = \delta_{ij}$ and a constant trace of the extrinsic curvature $K = \text{const}$. Quite remarkably, the resulting equations for the momentum constraints admit analytic solutions describing multiple black holes with nonvanishing spins and linear momenta [30]. There then remains a single elliptic differential equation, the Hamiltonian constraint, for the conformal factor ψ which requires a numerical treatment. By applying a compactification to the internal asymptotically flat region, Brandt & Brügmann [31] derived a method of solving the Hamiltonian constraint which is now generally referred to as the *puncture* method. These puncture data form the starting point for the majority of numerical simulations using the *moving-puncture* method [32,33]. We note that an alternative approach to evolving the Einstein equations based on the *generalized harmonic* formulation has been implemented with similar success [34,35].

As shown by Yoshino *et al.* [36], the existence of an analytic solution of the Bowen-York type for the momentum constraints carries over to the theory of general relativity in higher dimensions. These authors also solved the Hamiltonian constraint using a finite-difference method. Here, we will present a generalization of the spectral solver by Ansorg *et al.* [37], used inside the CACTUS toolkit [38,39], that solves the Hamiltonian constraint for black hole binaries in $D \geq 5$ dimensions with nonvanishing initial boost, and preserves the spectral convergence properties observed in four dimensions. The compactification implemented in this solver further facilitates direct interpolation of the initial data onto computational grids of arbitrary size with mesh refinement employed in state-of-the-art numerical simulations of black hole spacetimes. Finally, the initial data are generated in variables that can be straightforwardly translated to evolution systems common in numerical relativity, such as the Baumgarte-Shapiro-Shibata-Nakamura [40,41] system in Cartesian form. In our case, we specifically translate the spectral solution into the formalism of [13] which can thus be readily used to perform high-energy collisions of two black holes in D dimensions. We complement our study with the analytic perturbative analysis of boosted single puncture initial data.

This paper is organized as follows. In Sec. II, we review the constraint equations, the Brill-Lindquist [42] and Bowen-York [30] type initial data, and introduce an appropriate coordinate system. In Sec. III, we provide the explicit form of the elliptic equation that must be solved for determining the Bowen-York initial data that describes a boosted head-on collision in D dimensions. We also present its dimensional reduction to four spacetime dimensions, following [13]. In Sec. IV, the case of a single black hole with linear momentum is considered, and it is shown that an approximate analytic solution can be found for *all* variables, including the conformal factor, in the limit of small momentum to mass ratio. In Sec. V, we explain the modifications we have coded to study the case of two black holes with aligned linear momentum $P/r_S^{D-3} = \pm 0.8$ (r_S is the Schwarzschild radius) and present results for convergence tests, constraint violation, and the solution itself in $D = 4, 5, 6, 7$.

Notation: In the remainder of this work, early lower case Latin indices *a, b, c,* ... extend from 1 to $D-1$, late lower case Latin indices *i, j, k,* ... run from 1 to 3 and early upper case Latin indices *A, B, C,* ... from 4 to $D-1$.

II. HIGHER-DIMENSIONAL INITIAL DATA

The starting point for our discussion is a $(D-1)$-dimensional spacelike hypersurface $\bar{\Sigma}$ with induced metric $\bar{\gamma}_{ab}$, and extrinsic curvature $\bar{K}_{ab}$ embedded in a D-dimensional spacetime. By generalizing the ADM decomposition, the spacetime metric is given in the form

$$ds^2 = -\alpha^2 dt^2 + \bar{\gamma}_{ab}(dx^a + \beta^a dt)(dx^b + \beta^b dt). \tag{2.1}$$

We conformally decompose the spatial metric and extrinsic curvature as

$$\bar{\gamma}_{ab} = \psi^{(4/D-3)} \hat{\gamma}_{ab}, \qquad \bar{K}_{ab} = \psi^{-2} \hat{A}_{ab} + \frac{1}{D-1} \bar{\gamma}_{ab} \bar{K}, \tag{2.2}$$

which generalizes the $3+1$-dimensional Eq. (1.1). Note that we here represent the traceless part of the extrinsic curvature by the conformally rescaled version $\hat{A}^{ab}$. We assume that the conformal metric $\hat{\gamma}_{ab}$ is flat and impose the maximal slicing condition, $\bar{K} = 0$, which lead to the

decoupling of the constraints mentioned above. With this choice, the higher-dimensional initial data equations in vacuum become [36,43]

$$\partial_a \hat{A}^{ab} = 0, \tag{2.3}$$

$$\hat{\triangle}\psi + \frac{D-3}{4(D-2)}\psi^{-(3D-5)/(D-3)}\hat{A}^{ab}\hat{A}_{ab} = 0, \tag{2.4}$$

where $\hat{A}^{ab} \equiv \hat{\gamma}^{ac}\hat{\gamma}^{bd}\hat{A}_{cd}$, $\hat{\triangle} \equiv \partial_a\partial^a$ is the flat space Laplace operator and the first equation holds in a $(D-1)$-dimensional Cartesian frame $\mathcal{X}^a = (x^1, x^2, \ldots, x^{D-1})$.

A. Brill-Lindquist initial data

For the time-symmetric case $\bar{K}_{ab} = 0$, Eq. (2.3) is automatically satisfied, and Eq. (2.4) reduces to the $D-1$-dimensional flat space Laplace equation,

$$\hat{\triangle}\psi = 0. \tag{2.5}$$

For asymptotically flat spacetimes, the conformal factor satisfies the boundary condition

$$\lim_{r\to\infty}\psi = 1, \tag{2.6}$$

and a solution to Eq. (2.5) is given by

$$\psi = \psi_{\rm BL} = 1 + \sum_{i=1}^{N}\frac{\mu_{(i)}}{4r_{(i)}^{D-3}}, \tag{2.7}$$

where $r_{(i)} \equiv |r - x_{(i)}|$, $x_{(i)}$ is the (arbitrary) coordinate location of the ith puncture, and the mass parameter $\mu_{(i)}$ is related to the horizon radius $r_{S_{(i)}}$ and the ADM mass $M_{(i)}$ of the ith hole by

$$\mu_{(i)} \equiv r_{S_{(i)}}^{D-3} \equiv \frac{16\pi M_{(i)}}{\mathcal{A}_{D-2}(D-2)};$$

here $\mathcal{A}_{D-2}$ is the area of the unit $(D-2)$-sphere, and we have set the D dimensional Newton constant to unity.

These closed-form analytic data are the D-dimensional generalization of Brill-Lindquist data [42] and describe a spacetime containing multiple nonspinning black holes at the moment of time symmetry, *i.e.* with vanishing linear momentum.

B. Bowen-York initial data

In order to numerically evolve black holes with nonzero boost, we need to generalize Brill-Lindquist data to the non time-symmetric case. In four dimensions, this generalization is given by the Bowen-York extrinsic curvature, a nontrivial analytic solution of the momentum constraint Eq. (2.3). As shown by Yoshino *et al.* [36], we can write a solution of Eq. (2.3) describing a spacetime of arbitrary dimensionality D containing N black holes in the form

$$\hat{A}^{ab}_{P} = \sum_{i=1}^{N}\hat{A}^{ab}_{P(i)}, \tag{2.8}$$

where

$$\hat{A}^{ab}_{P(i)} = \frac{4\pi(D-1)}{(D-2)\mathcal{A}_{D-2}}\frac{1}{r_{(i)}^{D-2}}(n^a_{(i)}P^b_{(i)} + n^b_{(i)}P^a_{(i)} - (n_{(i)})_c P^c_{(i)}\hat{\gamma}^{ab} + (D-3)n^a_{(i)}n^b_{(i)}P^c_{(i)}(n_{(i)})_c). \tag{2.9}$$

Here we have introduced $n^a_{(i)} \equiv \frac{x^a - x^a_{(i)}}{r_{(i)}}$ and the parameter $P^a_{(i)}$ corresponds to the ADM momentum of the ith black hole in the limit of large separation from all other holes.

In order to obtain a complete set of initial data, we still need to solve the Hamiltonian constraint (2.3) with $\hat{A}_{ab}$ given by (2.8). For this purpose, we follow the standard decomposition of the conformal factor into a Brill-Lindquist contribution $\psi_{\rm BL}$ given by (2.7) plus a regular correction u

$$\psi = \psi_{\rm BL} + u. \tag{2.10}$$

Equation (2.4) then takes the form

$$\hat{\triangle}u + \frac{D-3}{4(D-2)}\hat{A}^{ab}\hat{A}_{ab}\psi^{-(3D-5)/(D-3)} = 0. \tag{2.11}$$

As in $D = 4$, the higher-dimensional extension of Bowen-York extrinsic curvature data can also accommodate angular momentum of the black holes. In the present work, however, we shall focus on initial data for nonspinning, boosted black holes only.

C. Coordinate transformation

In summary, the initial data are determined by (i) the extrinsic curvature $\bar{K}_{ab}$ obtained by inserting Eq. (2.9) into (2.8) and the resulting $\hat{A}_{ab}$ into Eq. (2.2), and (ii) the spatial $D-1$ metric $\bar{\gamma}_{ab}$ obtained by numerically solving Eq. (2.11) for u which gives the conformal factor via Eq. (2.10) and the metric through Eq. (2.2).

For the numerical solution of Eq. (2.11), it is convenient to transform to a coordinate system adapted to the generalized axial symmetry $SO(D-2)$ in $D = 5$ dimensions and $SO(D-3)$ in $D \geq 6$ dimensions as discussed in Sec. I C of Ref. [13]. For this purpose, we consider the (flat) conformal metric in cylindrical coordinates

$$\hat{\gamma}_{ab}dx^a dx^b = dz^2 + d\rho^2 + \rho^2(d\varphi^2 + \sin^2\varphi d\Omega_{D-4}), \tag{2.12}$$

where $d\Omega_{D-4}$ is the metric on the $(D-4)$-sphere. Observe that φ is a polar rather than an azimuthal coordinate, i.e. $\varphi \in [0, \pi]$. Next, following [13], we introduce "incomplete" Cartesian coordinates as

$$x = \rho\cos\varphi, \qquad y = \rho\sin\varphi, \tag{2.13}$$

where $-\infty < x < +\infty$ and $0 \le y < +\infty$. The D-dimensional initial data for the spatial metric is then

$$\bar{\gamma}_{ab}dx^a dx^b = \psi^{4/(D-3)}[dx^2 + dy^2 + dz^2 + y^2 d\Omega_{D-4}]. \tag{2.14}$$

We can transform the $D-1$-dimensional Cartesian coordinates $\mathcal{X}^a = (x^1, \ldots, x^{D-1})$ to the coordinate system $\mathcal{Y}^a = (x, y, z, \xi_1, \xi_2, \ldots, \xi_{D-4})$ with hyperspherical coordinates $\xi_1, \ldots, \xi_{D-4}$ by

$$\begin{aligned}
x^1 &= x \\
x^2 &= y\cos\xi_1 \\
x^3 &= z \\
x^4 &= y\sin\xi_1\cos\xi_2 && (D \ge 6) \\
x^5 &= y\sin\xi_1\sin\xi_2\cos\xi_3 && (D \ge 7) \\
&\vdots \\
x^{D-3} &= y\sin\xi_1\cdots\sin\xi_{D-6}\cos\xi_{D-5} && (D \ge 7) \\
x^{D-2} &= y\sin\xi_1\cdots\sin\xi_{D-5}\cos\xi_{D-4} && (D \ge 6) \\
x^{D-1} &= y\sin\xi_1\cdots\sin\xi_{D-4} && (D \ge 5).
\end{aligned} \tag{2.15}$$

Without loss of generality, we can always choose coordinates such that the black holes are initially located on the z-axis at z_1 and z_2 and have momenta of equal magnitude in opposite directions $P^a_{(1)} = -P^a_{(2)}$. Inserting the momenta into Eq. (2.9) then provides the conformal traceless extrinsic cuvature and the differential Eq. (2.11), which is solved numerically for u.

The class of symmetries covered by the formalism developed in Ref. [13] includes head-on and grazing collisions of nonspinning black holes with initial position and momenta

$$\begin{aligned}
x^a_{(1)} &= (0, 0, z_1, 0, \ldots, 0), \\
x^a_{(2)} &= (0, 0, z_2, 0, \ldots, 0) \\
P^a_{(1)} &= (P^x, 0, P^z, 0, \ldots, 0) = -P^a_{(2)}.
\end{aligned} \tag{2.16}$$

Note that a nonzero P^y is not compatible with the assumed symmetries. On the other hand, the x-axis can always be oriented such that the collision takes place in the xz-plane. Our formalism therefore covers general grazing collisions of nonspinning black hole binaries in D dimensions.

III. FOUR-DIMENSIONAL INITIAL DATA FOR A GENERAL D HEAD-ON COLLISION

For illustration and numerical testing, we will in the rest of this paper discuss in full detail the case of black holes with momenta in the z direction, that is, the case given by setting $P^x = 0$ in Eq. (2.16). The linear momenta are thus given by

$$P^a_{(1)} = (0, 0, P^z, 0, \ldots, 0) = -P^a_{(2)}. \tag{3.1}$$

The rescaled trace-free part of the extrinsic curvature for such a configuration is

$$\hat{A}_{ab} = \hat{A}^{(1)}_{ab} + \hat{A}^{(2)}_{ab}, \tag{3.2}$$

where $\hat{A}^{(1)}_{ab}$ and $\hat{A}^{(2)}_{ab}$ are given by Eq. (2.9) with (2.16) and (3.1). Using Eq. (2.15), we can write this in the coordinate system $\mathcal{Y}^a$ adapted to the spacetime symmetry:

$$\hat{A}^{(1)}_{ab} = \frac{4\pi(D-1)P^z}{(D-2)\mathcal{A}_{D-2}(x^2 + y^2 + (z-z_1)^2)^{(D+1)/2}} \begin{pmatrix} \hat{a}^{(1)}_{ij} & 0 \\ 0 & \hat{a}^{(1)}_{AB} \end{pmatrix}, \tag{3.3}$$

with

$$\hat{a}^{(1)}_{ij} = \begin{pmatrix} -[-(D-4)x^2 + y^2 + (z-z_1)^2](z-z_1) & (D-3)xy(z-z_1) & x[x^2 + y^2 + (D-2)(z-z_1)^2] \\ (D-3)xy(z-z_1) & -[x^2 - (D-4)y^2 + (z-z_1)^2](z-z_1) & y[x^2 + y^2 + (D-2)(z-z_1)^2] \\ x[x^2 + y^2 + (D-2)(z-z_1)^2] & y[x^2 + y^2 + (D-2)(z-z_1)^2] & [x^2 + y^2 + (D-2)(z-z_1)^2](z-z_1)) \end{pmatrix}, \tag{3.4}$$

and

$$\hat{a}^{(1)}_{AB} = -y^2(z-z_1)[x^2 + y^2 + (z-z_1)^2]h_{AB}, \tag{3.5}$$

where h_{AB} is the metric on the $(D-4)$-sphere. The expression for $\hat{A}^{(2)}_{ab}$ is analogous, but with z_2 in place of z_1 and $-P^z$ in place of P^z in Eq. (3.3).

The formalism developed in [13] for D-dimensional spacetimes with $SO(D-2)$ or $SO(D-3)$ isometries describes the spacetime in terms of the traditional three-dimensional metric γ_{ij} and extrinsic curvature K_{ij} coupled to a scalar field λ and its conjugate momentum K_λ; cf. Eqs. (2.14), (2.26) in [13]. These are the variables evolved in time and therefore the variables we ultimately wish to construct from the initial data calculation. For their extraction, we first note that γ_{ij}, K_{ij}, and K_λ are related to the $(D-1)$-dimensional metric $\bar{\gamma}_{ab}$ and extrinsic curvature $\bar{K}_{ab}$ by

$$\bar{\gamma}_{ij} = \gamma_{ij}, \qquad \bar{\gamma}_{AB} = \lambda h_{AB}, \qquad \bar{\gamma}_{iA} = 0, \tag{3.6}$$

$$\bar{K}_{ij} = K_{ij}, \qquad \bar{K}_{AB} = \frac{1}{2} K_\lambda h_{AB},$$
$$\bar{K}_{iA} = 0, \qquad \bar{K} = K + \frac{D-4}{2}\frac{K_\lambda}{\lambda}. \tag{3.7}$$

Using these relations and Eq. (2.14) of [13], we can express all "3 + 1" variables in terms of those describing the initial data

$$\gamma_{ij} = \psi^{4/(D-3)}\delta_{ij}, \qquad \lambda = \psi^{4/(D-3)} y^2,$$
$$K_{ij} = \psi^{-2}(\hat{A}^{(1)}_{ij} + \hat{A}^{(2)}_{ij}), \qquad K_\lambda = 2\psi^{-2} y^2 (P^+ + P^-),$$
$$K = -\frac{(D-4)K_\lambda}{2\lambda}, \tag{3.8}$$

where

$$P^+ \equiv -\frac{4\pi(D-1)P^z(z-z_1)}{(D-2)\mathcal{A}_{D-2}(x^2+y^2+(z-z_1)^2)^{(D-1)/2}},$$
$$P^- \equiv \frac{4\pi(D-1)P^z(z-z_2)}{(D-2)\mathcal{A}_{D-2}(x^2+y^2+(z-z_2)^2)^{(D-1)/2}}. \tag{3.9}$$

The conformal factor is

$$\psi = 1 + \frac{\mu_1}{4[x^2+y^2+(z-z_1)^2]^{(D-3)/2}} + \frac{\mu_2}{4[x^2+y^2+(z-z_2)^2]^{(D-3)/2}} + u, \tag{3.10}$$

and u is the solution of the equation

$$\left(\partial_{\rho\rho} + \partial_{zz} + \frac{D-3}{\rho}\partial_\rho\right)u = \frac{3-D}{4(D-2)}\hat{A}^{ab}\hat{A}_{ab}\psi^{-((3D-5)/(D-3))}, \tag{3.11}$$

where

$$\hat{A}^{ab}\hat{A}_{ab} = (\hat{A}^{(1)}_{ij} + \hat{A}^{(2)}_{ij})(\hat{A}^{ij(1)} + \hat{A}^{ij(2)}) + (D-4)(P^+ + P^-)^2. \tag{3.12}$$

Our numerical construction of the function u will be based on the spectral solver developed in [37]. This solver employs coordinates specifically adapted to the asymptotic behavior of u at spatial infinity. In order to investigate this behavior, we next consider a single black hole with nonzero linear momentum.

IV. SINGLE PUNCTURE WITH LINEAR MOMENTUM

For a single puncture with momentum P^z located at the origin $z = 0$ Eq. (2.9) implies

$$\hat{A}^{ab}\hat{A}_{ab} = \frac{16\pi^2(D-1)^2}{(D-2)^2\mathcal{A}^2_{D-2}r^{2(D-2)}}P_z^2 \times\left[2 + D(D-3)\left(\frac{z}{r}\right)^2\right], \tag{4.1}$$

so that Eq. (3.11) takes the form

$$\hat{\triangle}u + \frac{8\pi^2(D-1)^2(D-3)}{(D-2)^3\mathcal{A}^2_{D-2}r^{2(D-2)}}P_z^2 \times\left[1 + \frac{D(D-3)}{2}\left(\frac{z}{r}\right)^2\right]\psi^{-((3D-5)/(D-3))} = 0. \tag{4.2}$$

It turns out to be convenient for solving this differential equation to introduce a hyperspherical coordinate system on the $D-1$-dimensional spatial slices, such that the flat conformal metric is

$$d\hat{s}^2 = \hat{\gamma}_{ab}dx^a dx^b = dr^2 + r^2[d\vartheta^2 + \sin\vartheta^2(d\varphi^2 + \sin^2\varphi d\Omega_{D-4})],$$

with $\cos\vartheta = \frac{z}{r}$. We further introduce the radial coordinate

$$X \equiv \left(1 + \frac{\mu}{4r^{D-3}}\right)^{-1}, \tag{4.3}$$

which reduces to the coordinate A of Eq. (31) in [37] for the case of $D = 4$ spacetime dimensions. Expressed in the new coordinate system, Eq. (4.3) becomes

$$\left\{\partial_{XX} + \frac{2}{X}\partial_X + \frac{1}{(D-3)^2X^2(1-X)^2}\left[\partial_{\vartheta\vartheta} + (D-3)\cot\vartheta\partial_\vartheta + \frac{1}{\sin^2\vartheta}(\partial_{\varphi\varphi} + (D-4)\cot\varphi\partial_\varphi)\right]\right\}u = -\alpha\left(\frac{P_z}{\mu}\right)^2 X^{-((D-7)/(D-3))}(1+uX)^{-((3D-5)/(D-3))}\left(1 + \frac{D(D-3)}{2}\cos^2\vartheta\right), \tag{4.4}$$

with

$$\alpha \equiv \frac{128\pi^2(D-1)^2}{(D-3)(D-2)^3\mathcal{A}^2_{D-2}}.$$

For $D = 4$, we recover Eq. (40) of [37]. In order to study the behavior of the solution at spatial infinity, we now perform a Taylor expansion in $\upsilon \equiv \frac{P_z}{\mu}$,

$$u = \sum_{j=1}^{\infty}\upsilon^{2j}u_j. \tag{4.5}$$

Odd powers of υ have to vanish in order to satisfy Eq. (4.4). We have the following equation for u_1:

$$\left\{\partial_{XX}+\frac{2}{X}\partial_X+\frac{1}{(D-3)^2X^2(1-X)^2}[\partial_{\vartheta\vartheta}+(D-3)\cot\vartheta\partial_\vartheta]\right\}u_1=-\alpha X^{-((D-7)/(D-3))}\left(1+\frac{D(D-3)}{2}\cos^2\vartheta\right). \quad (4.6)$$

In order to solve Eq. (4.6), we make the *ansatz*

$$u_1=f(X)+g(X)Q_D(\cos\vartheta), \quad (4.7)$$

where $Q_D(\cos\vartheta)=(D-1)\cos^2\vartheta-1$. By solving Eq. (4.6), we find that the functions $f(X)$ and $g(X)$ take the form

$$f(X)=\frac{32\pi^2(D-3)}{(D-2)^2\mathcal{A}^2_{D-2}}(1-X^{((D+1)/(D-3))}), \quad (4.8)$$

$$\begin{aligned}g(X)=&\,k_1\left(\frac{X}{1-X}\right)^{(2/(D-3))}+k_2\left(\frac{1-X}{X}\right)^{((D-1)/(D-3))}-\alpha\frac{D(D-3)^3}{2(D+1)(D-1)}\\&\times\left[\frac{1}{D-1}\frac{X^{((D+1)/(D-3))}}{(1-X)^{(2/(D-3))}}{}_2F_1\left(-\frac{D-1}{D-3},\frac{D-1}{D-3};2\frac{D-2}{D-3};X\right)\right.\\&\left.-\frac{1}{2D}X^{((D+1)/(D-3))}(1-X)^{((D-1)/(D-3))}_2{}_2F_1\left(\frac{2}{D-3},\frac{2D}{D-3};3\frac{D-1}{D-3};X\right)\right],\end{aligned} \quad (4.9)$$

where ${}_2F_1(a,b;c;X)$ is the hypergeometric function and $k_{1,2}$ are constants to be fixed by imposing that $g(X=1)=0$ and $g(X=0)$ is smooth. Requiring analyticity at $X=0$ and using the property $F(a,b,c,0)=1$, we immediately find $k_2=0$.

We are now interested in the large $X\to 1$ limit. Therefore, we use the $z\to 1-z$ transformation law for the hypergeometric functions [44],

$$\begin{aligned}F(a-c+1,b-c+1,2-c,z)=&\,(1-z)^{c-a-b}\frac{\Gamma(2-c)\Gamma(a+b-c)}{\Gamma(a-c+1)\Gamma(b-c+1)}F(1-a,1-b,c-a-b+1,1-z)\\&+\frac{\Gamma(2-c)\Gamma(c-a-b)}{\Gamma(1-a)\Gamma(1-b)}F(a-c+1,b-c+1,-c+a+b+1,1-z).\end{aligned} \quad (4.10)$$

Requiring a regular solution, we find that k_1 has to satisfy

$$k_1=\frac{64\pi^2D(D-3)^2}{(D-2)^3(D+1)\mathcal{A}^2_{D-2}}\frac{\Gamma(\frac{2(D-2)}{D-3})^2}{\Gamma(\frac{3D-5}{D-3})}. \quad (4.11)$$

Let us write these functions explicitly for $D=4,5,7$ (for $D=6$ the hypergeometric function does not simplify):

(i) $D=4$:

$$f(X)=\frac{1}{2}(1-X^5), \quad (4.12)$$

$$\begin{aligned}g(X)=&\,\frac{(1-X)^2}{10X^3}[84(1-X)\log(1-X)+84X\\&-42X^2-14X^3-7X^4-4X^5-2X^6].\end{aligned} \quad (4.13)$$

These are Eqs. (42–44) in [37], with appropriate redefinitions.

(ii) $D=5$:

$$f(X)=\frac{16}{9\pi^2}(1-X^3), \quad (4.14)$$

$$\begin{aligned}g(X)=&-\frac{80(1-X)^2}{81\pi^2X^2}[4\log(1-X)+4X\\&+2X^2+X^3];\end{aligned} \quad (4.15)$$

(iii) $D=7$:

$$f(X)=\frac{128(1-X^2)}{25\pi^4}, \quad (4.16)$$

$$\begin{aligned}g(X)=&\,\frac{28}{125\pi^4\sqrt{(1-X)X^3}}\\&\times[-30\sqrt{(1-X)X}+40\sqrt{(1-X)X^3}\\&-16\sqrt{(1-X)X^7}+3\pi X^2\\&+6(5-10X+4X^2)\arcsin\sqrt{X}].\end{aligned} \quad (4.17)$$

Analyzing these expressions, we can anticipate the convergence properties of the numerical solutions obtained in terms of pseudospectral methods. For instance, analyticity of f and g suggests exponential convergence. As will become clear in the next section, we are interested in the convergence properties in a coordinate A behaving as $A\sim 1-\frac{1}{r}$, for large r. We thus introduce a coordinate A that satisfies

$$X = (1 + (A^{-1} - 1)^{D-3})^{-1}. \tag{4.18}$$

In terms of the A coordinate, we find that the functions f are analytical. For the function g in the vicinity of $A = 1$, the leading terms behave as follows:

(i) $D = 5$

$$g(A) \sim -\frac{80}{81\pi^2}(1-A)^4[8\log(1-A) + 7], \tag{4.19}$$

(ii) $D = 6$

$$g(A) \sim \frac{19\,683}{6272\pi^2}(1-A)^5, \tag{4.20}$$

(iii) $D = 7$

$$g(A) \sim \frac{84}{25\pi^3}(1-A)^6. \tag{4.21}$$

From the behavior of the functions f and g and Eq. (4.7), we conclude that the first term in the expansion (4.5) has a leading-order behavior $u_1 \sim 1/r^{D-3}$ as $r \to \infty$. Iteratively solving Eq. (4.4) for higher powers of υ is complicated by the presence of the source terms on the right-hand side, but under simplifying assumptions indicates that higher-order terms $u_j \geq 2$ acquire additional factors of $1/r$ and therefore the leading-order falloff behavior is given correctly by that of u_1. This result is confirmed by our numerical investigation using finite-boost parameters as we shall discuss in the next section.

With regard to the analyticity of the solutions and the resulting expectations for the convergence properties of a spectral algorithm, we summarize the results of our analytical study of a single puncture as follows. In $D = 6, 7$, the leading terms are analytic functions in the vicinity of $A = 1$. Actually, for $D = 7$, $g(A)$ is analytic in the vicinity of any point. Therefore, we expect exponential convergence of the pseudospectral code. For $D = 5$, one observes the presence of a logarithmic term. This type of term is known to arise in $D = 4$, when punctures have nonvanishing momenta [45,46] and in that case their presence makes the convergence algebraic in the single puncture case. In the next section, we shall investigate the impact of the logarithmic terms on the convergence properties of our spectral solver.

V. TWO PUNCTURES WITH LINEAR MOMENTUM

A. Code changes

We first explicitly list the modifications applied to the spectral solver of Ref. [37] and demonstrate how these modifications enable us to generate initial data for boosted black hole binaries with convergence properties and levels of constraint violation similar to the $D = 4$ case. For this purpose, we start by recalling that the spectral solver of [37] employs coordinates

$$A \in [0, 1], \qquad B \in [-1, 1], \qquad \phi \in [0, 2\pi], \tag{5.1}$$

which are defined by Eq. (62) of [37],

$$\begin{aligned} x &= b\frac{2A}{1-A^2}\frac{1-B^2}{1+B^2}\sin\phi, \\ y &= b\frac{2A}{1-A^2}\frac{1-B^2}{1+B^2}\cos\phi, \\ z &= b\frac{A^2+1}{A^2-1}\frac{2B}{1+B^2}, \end{aligned} \tag{5.2}$$

where b is half of the coordinate distance between the punctures. In particular, the coordinate A satisfies

$$r \to \infty \Leftrightarrow A \to 1. \tag{5.3}$$

The first modification consists in adapting the source term and Laplace operator according to (3.11).

Next, we note that the type of high-energy collisions which form the main motivation for this work often start from relatively large initial separations of the holes, $|z_1 - z_2| \gg r_S$. In order to obtain high-precision solutions for such binary configurations, we found it crucial to introduce a coordinate A' defined as

$$A = \frac{\sinh[\kappa(A'+1)/2]}{\sinh\kappa}, \tag{5.4}$$

where κ is an adjustable free parameter. Note that for $\kappa = 0$ we obtain $A = \frac{1}{2}(A' + 1)$. For $\kappa > 0$, however, the new coordinate A' provides the spectral method with enhanced resolution near $A \sim 0$.

A further modification is related to the asymptotic falloff of the function u as obtained in the previous section,

$$u \sim \frac{1}{r^{D-3}}. \tag{5.5}$$

To naturally accommodate this behavior with the spectral coordinates used in the code, we have changed the variable U of Eq. (5) in [37] to

$$u = (A' - 1)^{D-3}U. \tag{5.6}$$

Note that this U variable is the variable that the code actually solves for.

Finally, we adjust the calculation of the ADM mass from the numerical solution. For this purpose, we note that, asymptotically

$$\psi = 1 + \frac{\mu_+}{4r_+^{D-3}} + \frac{\mu_-}{4r_-^{D-3}} + u \sim 1 + \frac{\mu}{4r^{D-3}}, \tag{5.7}$$

with $\mu \equiv r_{S_{\text{global}}}^{D-3} \equiv \frac{16\pi M_{\text{ADM}}}{\mathcal{A}_{D-2}(D-2)}$ and $\mu_\pm \equiv r_{S_{(\pm)}}^{D-3}$. The ADM mass is then obtained from

TABLE I. ADM mass obtained with Eq. (5.8) in units of the "bare" Schwarzschild radius $r_S^{D-3} = r_{S_{(+)}}^{D-3} + r_{S_{(-)}}^{D-3}$. The variation of the ADM mass with resolution is of the order of 10^{-10} for all D and $n \geq 100$ grid points indicating that the accuracy in the ADM mass is limited by round-off errors.

D	b/r_S	P/r_S^{D-3}	$r_{S_{\rm global}}^{D-3}/r_S^{D-3}$	$M_{\rm ADM}/r_S^{D-3}$
4	30.185	0.8	3.555	1.78
5	30.185	0.8	1.931	2.27
6	30.185	0.8	1.415	2.96
7	30.185	0.8	1.236	3.81

$$r_{S_{\rm global}}^{D-3} = r_{S_{(+)}}^{D-3} + r_{S_{(-)}}^{D-3} + 4\lim_{r\to\infty} r^{D-3}u$$
$$= r_{S_{(+)}}^{D-3} + r_{S_{(-)}}^{D-3} + 4\left(-2b\frac{\tanh\kappa}{\kappa}\right)^{D-3} U(A'=1), \tag{5.8}$$

where we have used Eq. (62) of [37], and Eq. (5.4) and (5.6). We show in Table I the values obtained for the ADM mass of some cases we considered.

B. Results

We now study the numerical results as obtained for $D = 4, 5, 6, 7$ with these adaptations of the spectral solver of [37]. Throughout the remainder of this section, we will graphically present results in units of the "bare" Schwarzschild radius defined as $r_S^{D-3} = r_{S_{(+)}}^{D-3} + r_{S_{(-)}}^{D-3}$.

We first address the convergence properties of the numerical algorithm by evaluating the quantity

$$\delta_{n,m}(u) = \max|1 - u_n/u_m|, \tag{5.9}$$

where the maximum is obtained along the collision axis, i.e. z-axis in our case. Here, the index m refers to a reference solution obtained using a large number m of grid points while n denotes test solutions using a coarser resolution, $n < m$. The result obtained for black hole binaries with initial separation $b/r_S = 30.185$ and boost $P^z/r_S^{D-3} = 0.8$ in $D = 4, 5, 6$ and 7 dimensions is displayed in Fig. 1. We note from this figure, that achieving a given target accuracy $\delta_{n,m}$ requires a larger number of points n as D increases. We emphasize in this context, however, that this increase in computational cost in higher dimensions is unlikely to significantly affect the total computational cost of the simulations which typically are dominated by the time evolution rather than the initial data calculation. Most importantly, we observe exponential convergence up to a level of $\delta_{n,m}(u) \approx 10^{-6}$ for all values of the spacetime dimensionality D. Below that level, the two leftmost curves in Fig. 1, corresponding to $D = 4$ and $D = 5$, respectively, show that the rate of convergence decreases indicating that the logarithmic terms become significant and reduce the convergence to algebraic level similar to the observation in Fig. 4 of Ref. [37]. For $D = 6$,

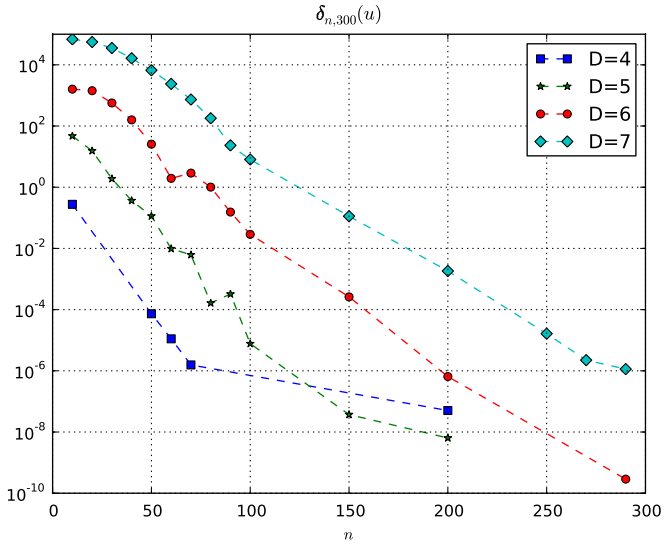

FIG. 1 (color online). Convergence plot for the $b/r_S = 30.185$, $P/r_S^{D-3} = \pm 0.80$ cases.

the convergence remains exponential, in agreement with the absence of logarithmic terms in the analysis of Sec. IV. Irrespective of a change to algebraic convergence, however, our algorithm is capable of reducing the quantity $\delta_{m,n}(u)$ for all values of D to a level comparable to the case $D = 4$ and, thus, producing initial data of similar quality as in $3 + 1$ dimensions, provided we use a sufficiently high resolution n.

For illustration, we plot in Fig. 2 the function u obtained for the case of $b/r_S = 30.185$, $P^z/r_S^{D-3} = 0.8$. The behavior is qualitatively similar for all values of D, but the figure demonstrates the faster falloff for larger D as predicted by (5.5). For this plot, we have used $n_A = 300$, $n_B = 300$

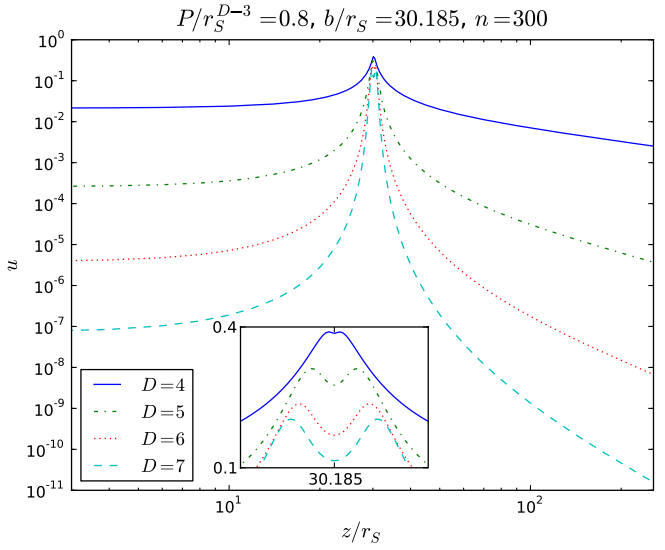

FIG. 2 (color online). u function for $D = 4, \ldots, 7$ plotted along the z-axis, in units of r_S. We used $n_A = n_B = n = 300$, $n_\phi = 4$. We also show a zoom around the puncture.

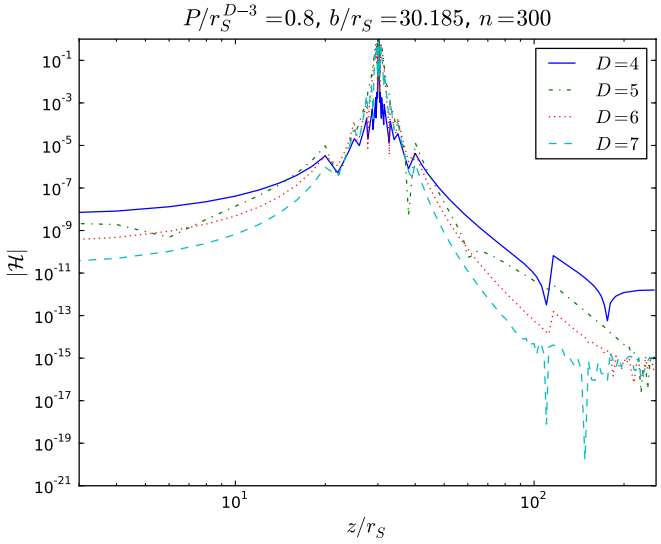

FIG. 3 (color online). Violation of the Hamiltonian constraint along the z-axis, evaluated with a fourth-order finite-difference scheme. The growth of the constraint violation near the puncture is an artifact of finite-differencing across the puncture; see text for details.

and $n_\phi = 4$ grid points. The inset in the figure shows the function u in the immediate vicinity of the puncture. While the profile develops multiple extrema for $D > 4$, the profile remains smooth for all values of D.

Finally, we show in Fig. 3, the Hamiltonian constraint corresponding to the solutions presented in Fig. 2 as measured by a fourth-order finite-differencing scheme of the evolution code [47]. We emphasize that the violation of Eq. (2.11) inside the spectral initial data solver is $<10^{-12}$ by construction. The independent evaluation of the constraint violation in the evolution code serves two purposes. First, it checks that the differential Eq. (2.11) solved by the spectral method corresponds to the Hamiltonian constraint formulated in ADM variables; an error in coding up the differential Eq. (2.11) could still result in a solution for u of the spectral solver but would manifest itself in significantly larger violations in Fig. 3. Second, it demonstrates that the remaining numerical error is dominated by the time evolution instead of the initial solver. Note in this context that the relatively large violations of order unity near the puncture location in Fig. 3 are an artifact of the fourth-order discretization in the diagnostics of the evolution code and are typical for evolutions of the moving-puncture type; see e. g. the right panel in Fig. 8 in Brown *et al.* [48].

The solid (blue) curve obtained for the "standard" $D = 4$ case serves as reference. For all values of D, the constraint violations are maximal at the puncture location $z_1/r_S \approx 15$ and rapidly decrease away from the puncture. As expected from the higher falloff rate of the grid functions for larger D, the constraints also drop faster for higher dimensionality of the spacetime.

VI. CONCLUSIONS

In this paper, we have presented numerical solutions of the Einstein constraint equations for the construction of initial data containing single or binary black holes with nonvanishing linear momentum in $D > 4$-dimensional spacetimes. For this purpose, we have modified the spectral solver of Ref. [37]. As in $D = 4$ dimensions, the momentum constraints decouple from the Hamiltonian constraint under the assumption of conformal flatness and a spatially constant trace of the extrinsic curvature and allow for an analytic solution describing multiple black holes with nonzero momenta. One thus arrives at a single elliptic differential equation for the conformal factor or, to be more specific, a regular correction function u to the Brill-Lindquist part of the conformal factor. We have studied the resulting differential equation in the limit of a single black hole with small boost in order to investigate the asymptotic behavior of u at spatial infinity, where we find $u \sim 1/r^{D-3}$. For $D = 6, 7$ we further observe that u is an analytic function expanded in terms of the coordinate A [cf. Eq. (4.18)] around spatial infinity, so that a spectral algorithm should provide exponential convergence. For $D = 5$, the expansion of u includes a logarithmic term, but, as has also been observed in Ref. [37] for $D = 4$, this term is subdominant in the case of a black hole binary with equal and opposite momenta. We have used the asymptotic behavior of u to adapt the set of coordinates employed in the spectral solver to arbitrary dimensionality and further performed a transformation to a radial coordinate that ensures sufficient resolution near spatial infinity for the case of large separation of the two holes.

The resulting code has been used to calculate initial data for black hole binaries with linear momenta along the z-axis, i.e. corresponding to a head-on collision. Even though the number of grid points required for reaching a given threshold accuracy increases with D, we observe rapid convergence for all values $D = 4, 5, 6, 7$. Although for large resolutions n the convergence becomes algebraic due to logarithmic terms in the r dependency of the solution u for $D = 4$ and $D = 5$, this transition can be compensated with a moderate increase in the number of grid points n as has also been observed in Ref. [37] for $D = 4$. Closer investigation of the profile of the function u thus obtained confirms the expected higher falloff rate as $r \to \infty$ for larger D. We further note that u shows smooth behavior near the puncture. Finally, we have studied the Hamiltonian constraint as a function along the collision axis. As in $D = 4$, the residual constraint violations after the elliptic solving are largest near the puncture and rapidly fall off away from the puncture. As expected from the asymptotic behavior of u, the constraint violations decay even faster away from the puncture as D increases.

The construction of initial data forms a crucial step in performing high-energy collisions of black hole binaries in higher-dimensional spacetimes which will complement

existing studies in $D = 4$ dimensions [18–20] as well as studies in $D = 5$ dimensions [17] starting from superposed single black hole initial data.

ACKNOWLEDGMENTS

We thank Andrea Nerozzi and the anonymous referee for useful suggestions and discussions. M. Z. and H. W. are funded by FCT through Grants No. SFRH/BD/43558/2008 and SFRH/BD/46061/2008. U. S. acknowledges support from the Ramón y Cajal Programme of the Ministry of Education and Science of Spain, the FP7-PEOPLE-2011-CIG Grant CBHEO, No. 293412, NSF grants PHY-0601459, PHY-0652995, and the Sherman Fairchild Foundation to Caltech. This work was supported by the DyBHo–256667 ERC Starting Grant and by FCT—Portugal through projects PTDC/FIS/098025/2008, PTDC/FIS/098032/2008, PTDC/CTE-AST/098034/2008, and CERN/FP/116341/2010. This research was supported by an allocation through the TeraGrid Advanced Support Program under Grant No. PHY-090003, an allocation by the Centro de Supercomputación de Galicia (CESGA) under project ICTS-2009-40 and allocations at the Barcelona Supercomputing Center (BSC) under projects AECT-2011-2-0006 and AECT-2011-2-0015. Computations were performed on the TeraGrid clusters Kraken at the National Institute for Computational Sciences (NICS) of the University of Tennessee and Trestles at the San Diego Supercomputing Center (SDSC), the Milipeia cluster in Coimbra, Finis Terrae at the Supercomputing Center of Galicia (CESGA), the supercomputer Caesaraugusta at the Institute for Biocomputation and Physics of Complex Systems (BIFI) at the University of Zaragoza, HLRB2 of the Landesrechenzentrum (LRZ) in Munich, MareNostrum at the Barcelona Supercomputing Center in Barcelona, and on the Blafis cluster at the University of Aveiro.

[1] I. Antoniadis, Phys. Lett. B **246**, 377 (1990).
[2] I. Antoniadis, N. Arkani-Hamed, S. Dimopoulos, and G. R. Dvali, Phys. Lett. B **436**, 257 (1998).
[3] L. Randall and R. Sundrum, Phys. Rev. Lett. **83**, 3370 (1999).
[4] P. C. Argyres, S. Dimopoulos, and J. March-Russell, Phys. Lett. B **441**, 96 (1998).
[5] T. Banks and W. Fischler, arXiv:hep-th/9906038.
[6] S. B. Giddings and S. D. Thomas, Phys. Rev. D **65**, 056010 (2002).
[7] S. Dimopoulos and G. L. Landsberg, Phys. Rev. Lett. **87**, 161602 (2001).
[8] E.-J. Ahn, M. Cavaglia, and A. V. Olinto, Phys. Lett. B **551**, 1 (2003).
[9] A. Chamblin, F. Cooper, and G. C. Nayak, Phys. Rev. D **70**, 075018 (2004).
[10] P. Kanti, Lect. Notes Phys. **769**, 387 (2009).
[11] H. Yoshino and M. Shibata, Phys. Rev. D **80**, 084025 (2009).
[12] E. Sorkin and M. W. Choptuik, Gen. Relativ. Gravit. **42**, 1239 (2010).
[13] M. Zilhao *et al.*, Phys. Rev. D **81**, 084052 (2010).
[14] L. Lehner and F. Pretorius, Phys. Rev. Lett. **105**, 101102 (2010).
[15] H. Witek, M. Zilhao, L. Gualtieri, V. Cardoso, and C. Herdeiro *et al.*, Phys. Rev. D **82**, 104014 (2010).
[16] H. Witek, V. Cardoso, L. Gualtieri, C. Herdeiro, and U. Sperhake *et al.*, Phys. Rev. D **83**, 044017 (2011).
[17] H. Okawa, K.-i. Nakao, and M. Shibata, Phys. Rev. D **83**, 121501 (2011).
[18] U. Sperhake, V. Cardoso, F. Pretorius, E. Berti, and J. A. Gonzalez, Phys. Rev. Lett. **101**, 161101 (2008).
[19] M. Shibata, H. Okawa, and T. Yamamoto, Phys. Rev. D **78**, 101501 (2008).
[20] U. Sperhake *et al.*, Phys. Rev. Lett. **103**, 131102 (2009).
[21] U. Sperhake, E. Berti, V. Cardoso, F. Pretorius, and N. Yunes, Phys. Rev. D **83**, 024037 (2011).
[22] R. Arnowitt, S. Deser, and C. W. Misner, Gen. Relativ. Gravit. **40**, No. 9, 1997 (2008).
[23] J. W. York, Jr., in *Sources of Gravitational Radiation*, edited by. L. L. Smarr (Cambridge University Press, Cambridge, 1979), p. 83.
[24] A. Lichnerowicz, J. Math. Pures Appl. **23**, 37 (1944).
[25] J. W. York, Jr., Phys. Rev. Lett. **26**, 1656 (1971).
[26] J. W. York, Jr., Phys. Rev. Lett. **28**, 1082 (1972).
[27] J. W. York, Jr., J. Math. Phys. (N.Y.) **14**, 456 (1973).
[28] G. B. Cook, Living Rev. Relativity **3**, 5 (2000).
[29] M. Alcubierre, *Introduction to 3+1 Numerical Relativity*, International Series of Monographs on Physics (Oxford University, New York, 2008).
[30] J. M. Bowen and J. W. York, Jr., Phys. Rev. D **21**, 2047 (1980).
[31] S. Brandt and B. Brügmann, Phys. Rev. Lett. **78**, 3606 (1997).
[32] M. Campanelli, C. O. Lousto, P. Marronetti, and Y. Zlochower, Phys. Rev. Lett. **96**, 111101 (2006).
[33] J. G. Baker, J. Centrella, D.-I. Choi, M. Koppitz, and J. van Meter, Phys. Rev. Lett. **96**, 111102 (2006).
[34] F. Pretorius, Phys. Rev. Lett. **95**, 121101 (2005).
[35] M. A. Scheel, M. Boyle, T. Chu, L. E. Kidder, K. D. Matthews, and H. P. Pfeiffer, Phys. Rev. D **79**, 024003 (2009).
[36] H. Yoshino, T. Shiromizu, and M. Shibata, Phys. Rev. D **74**, 124022 (2006).
[37] M. Ansorg, B. Bruegmann, and W. Tichy, Phys. Rev. D **70**, 064011 (2004).
[38] G. Allen, T. Goodale, J. Massó, and E. Seidel, in *Proceedings of Eighth IEEE International Symposium on High Performance Distributed Computing, HPDC-8, Redondo Beach, 1999* (IEEE, New York, 1999).

[39] Cactus Computational Toolkit, http://www.cactuscode.org.
[40] M. Shibata and T. Nakamura, Phys. Rev. D **52**, 5428 (1995).
[41] T. W. Baumgarte and S. L. Shapiro, Phys. Rev. D **59**, 024007 (1998).
[42] D. R. Brill and R. W. Lindquist, Phys. Rev. **131**, 471 (1963).
[43] H. Yoshino, T. Shiromizu, and M. Shibata, Phys. Rev. D **72**, 084020 (2005).
[44] M. Abramowitz and I. A. Stegun, *Handbook of Mathematical Functions with Formulas, Graphs, and Mathematical Tables* (Dover, New York, 1964), 5th ed.
[45] S. Dain and H. Friedrich, Commun. Math. Phys. **222**, 569 (2001).
[46] R. J. Gleiser, G. Khanna, and J. Pullin, Phys. Rev. D **66**, 024035 (2002).
[47] U. Sperhake, Phys. Rev. D **76**, 104015 (2007).
[48] D. Brown, P. Diener, O. Sarbach, E. Schnetter, and M. Tiglio, Phys. Rev. D **79**, 044023 (2009).